Modeling Three-Phase Grid-Connected Inverter System using Complex Vector in Synchronous *dq* Reference Frame and Analysis on the Influence of Tuning Parameters of Synchronous Frame PI Controller

Wooyoung Choi, *Student Member*, *IEEE*, Woongkul Lee, *Student Member*, *IEEE*, Casey Morris, and Bulent Sarlioglu, *Senior Member*, *IEEE*
Electrical and Computer Engineering
Wisconsin Electric Machines and Power Electronics Consortium (WEMPEC)
University of Wisconsin-Madison
Madison, WI 53706 USA
sarlioglu@wisc.edu

***Abstract*—This paper presents a mathematical modeling of three-phase grid-connected inverter system including output LCL filter and closed loop control using complex vector notation. The control scheme used is synchronous frame PI control on complex space vector of grid current in synchronous *dq* reference frame. Effect of controller's tuning parameters is investigated using complex vector root locus and complex vector frequency response function of closed loop system according to different tuning parameters. Control scheme and three-phase grid-connected inverter are simulated using MATLAB Simulink and SimPowerSystems ™.**

***Index Terms*—Grid-connected inverter, grid current control, and synchronous frame PI controller.**

I. INTRODUCTION

As renewable energy resources have continued to penetrate the modernized power system, the role of grid-connected inverters (GCIs) has become more important as an interface between distributed energy resources (DERs) and the grid. To achieve the desired performance of DERs, the controller of the GCI should be designed properly.

There are different methods introduced in literature regarding current controller of PWM inverters. Various control methods of GCI for renewable energy resources are reviewed in [1]. Reference [2] compares different multi-loop control strategies for voltage-source and current-source inverters. A comparison in terms of steady state and transient performance is done for different sensing positions in uninterrupted power supply (UPS) system in [3]. In reference [4], stationary and synchronous frame PI regulators are compared in frequency domain for current-regulated voltage-source inverters. Limitations of voltage-oriented PI control in stationary reference frame are discussed in [5]. Reference [6] states proportional and resonant regulator for PWM inverter, which brings about zero steady-state error. In reference [7], synchronous frame PI regulator is used for three-phase voltage-source inverter when there are inner control loop on filter capacitor current and outer control loop on grid current. Current regulators designed for ac load and motor using complex vector are introduced in [8, 9] and virtually translation technique is also applied for ac machine to further improve regulation performance [10]. Digital control is designed for three-phase inverter to achieve high power quality [11] and tuning method using pole place strategy is proposed in z-domain [12]. When faults occur, the control methods in different reference frames and control strategies are presented in [13].

GCI is modeled as *dq* model using scalar notation and synchronous frame PI controller is commonly used for GCI. It is difficult to analyze a GCI system and to tune the gains of PI controller when scalar notation is used. By using complex vector notation, the order of the system is reduced and it becomes easier to design the controller and analyze the system. Also, complex vector model is widely used in controlling ac machines. However, it has not been implemented much for GCI modeling. There are still opportunities to investigate the effect of tuning parameter to avoid instability and obtain high grid current quality when GCI is modeled using complex vector notation.

This paper presents a complex vector modeling of GCI with synchronous frame PI controller on grid current in synchronous *dq* reference frame. Also, the influence of controller's tuning parameters is investigated using complex vector root locus and complex vector frequency response function for three-phase GCI. The advantage of using complex vector notation when modeling GCI is introduced. Closed

978-1-5090-0261-0/16/$31.00 ©2016 IEEE

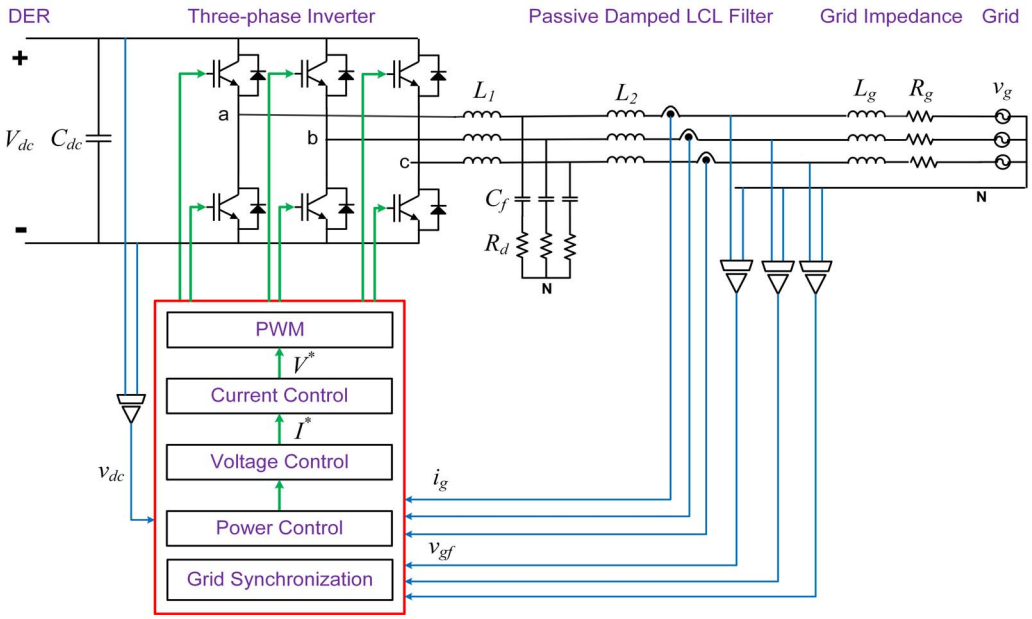

Fig. 1. Control scheme of grid-connected inverter system for three-phase four-wire grid.

loop transfer function of three-phase GCI including synchronous frame PI controller is derived as complex vector format.

II. Grid-Connected Inverter System

The GCI system consists of three-phase inverter, output LCL filter, the grid, and controller as shown in Fig. 1, which shows control scheme of grid-connected inverter system for three-phase four-wire grid. According to the objective of GCI, there can be different control loops to achieve the desired performance.

The GCI can be operated as current-controlled or voltage-controlled source according to different operation mode. Voltage-controlled is applied to grid supporting, micro-grid, and stand-alone modes. Current-controlled regulation is commonly used in grid-connected mode and has advantages such as fast response and better stability. In this paper, current controlled GCI is considered. Current-controlled voltage source inverters are used for GCIs in order to transfer power produced by DER to the grid as well as for inverter-based active shunt compensators to mitigate power quality problems.

Grid current quality is equally as important as grid voltage quality. According to IEEE 1547, total harmonic distortion (THD) of current injected to the grid should be less than 5%. Therefore, the performance of current regulator is significant to achieve balanced and sinusoidal three-phase grid current with low THD.

Commonly, control is two cascaded loops with a fast inner loop on current to regulate current and outer loop on voltage to regulate dc link voltage. Current controller is an inner loop of overall closed loop controller and gives voltage command to PWM. A current control loop is important to bring about high grid current quality in grid-connected mode. Current control can be designed in stationary or synchronous reference frame.

III. Complex Vector Modeling of Three-Phase Grid-Connected Inverter

Complex space vector of three-phase AC current in stationary reference frame is defined as (1) using complex vector notation.

$$\underline{i}^{s}_{abc}(t) = \sqrt{\frac{2}{3}}\left[i_a(t) + \underline{\alpha}\, i_b(t) + \underline{\alpha}^2 i_c(t) \right] \tag{1}$$

This complex space vector rotates forward or backward depending on sign of frequency.

The coefficient, $\underline{\alpha}$, is defined as (2) and has property of (3)

$$\underline{\alpha} = e^{j2\pi/3} \tag{2}$$

$$1 + \underline{\alpha} + \underline{\alpha}^2 = 0 \tag{3}$$

Three-phase voltage can also be represented as complex space vector in stationary reference frame as represented in (1).

Here, superscript *s* means that variable is represented in stationary reference frame and bar under variable means complex space vector. Subscripts a, b, or c represent phase A, B, or C of current.

Complex space vector of balanced three-phase currents with amplitude of I is represented in stationary reference frame as

$$\underline{i}^{s}_{abc}(t) = \sqrt{\frac{3}{2}} I e^{j\omega t} \tag{4}$$

where ω is the angular frequency of the grid and defined as

$$\omega = 2\pi f_g \tag{5}$$

Here, the frequency of the grid, f_g, is 60 Hz.

By using coordinate transformation, complex space vector of three-phase current in stationary reference frame is transformed into the complex space vector in synchronous *dq* reference frame written as

$$\underline{i}^{e}_{dq}(t) = e^{-j\omega t}\underline{i}^{s}_{abc}(t) = i_d(t) + ji_q(t) \tag{6}$$

where superscript *e* indicates that the variable is represented in synchronous *dq* reference frame, subscripts d and q represent d- and q-axis component of complex vector of three-phase current in synchronous *dq* reference frame, respectively.

Complex space vector of balanced three-phase currents in stationary reference frame is expressed as complex space vector in synchronous *dq* reference frame using (6). A purely sinusoidal current does not have imaginary component and only has d-axis component as shown in (7).

$$\underline{i}^{e}_{dq}(t) = \sqrt{\frac{3}{2}}I \tag{7}$$

This is one of the benefits of representing the three-phase current as complex vector in synchronous *dq* reference frame that d- and q-axis components of current are dc quantities for balanced current or voltage.

Using (1) and (6), three-phase GCI with output LCL filter and the grid can be modeled as complex vector in stationary reference frame or synchronous *dq* reference frame.

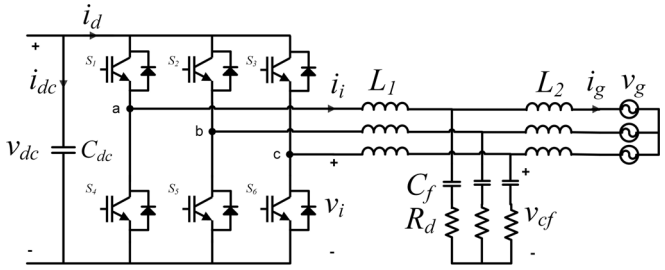

Fig. 2. A circuit diagram of three-phase GCI with LCL output filter and grid.

Fig. 2 show circuit diagram of three-phase GCI with LCL output filter and the grid. Grid impedance and equivalent resistances of output filter are neglected for simplicity.

v_{dc} is dc link voltage, C_{dc} is dc link capacitor, i_{dc} is dc link current flowing through dc link capacitor, and i_d is current flowing into the inverter. v_i is inverter output voltage, i_i is inverter output current, v_{cf} is voltage across filter capacitor, and i_g is grid current. L_1 is inverter-side inductor of LCL filter, L_2 is grid-side inductor of filter, C_f is filter capacitor of filter, and R_d is damping resistance. Due to the absence of grid impedance, point of common coupling (PCC) voltage, v_{gf} in Fig. 1 is identical to grid voltage.

State space equation of three-phase GCI in stationary reference frame is shown as (8). Subscript x stands for phase A, B, or C. State space equation can be written for each phase in stationary reference frame.

$$\begin{aligned}
\frac{d}{dt}i_{i,x}(t) &= \frac{1}{L_1}\left[v_{i,x}(t) - v_{cf,x}(t)\right] \\
\frac{d}{dt}v_{cf,x}(t) &= \left(\frac{1}{C_f} + R_d\frac{d}{dt}\right)\left[i_{i,x}(t) - i_{g,x}(t)\right] \\
\frac{d}{dt}i_{g,x}(t) &= \frac{1}{L_2}\left[v_{cf,x}(t) - v_{g,x}(t)\right]
\end{aligned} \tag{8}$$

Using (1), this can be expressed as complex vector form in stationary reference frame as

$$\begin{cases}
\frac{d}{dt}\underline{i}^{s}_{i,abc}(t) = \frac{1}{L_1}\left[\underline{v}^{s}_{i,abc}(t) - \underline{v}^{s}_{cf,abc}(t)\right] \\
\frac{d}{dt}\underline{v}^{s}_{cf,abc}(t) = \left(\frac{1}{C_f} + R_d\frac{d}{dt}\right)\left[\underline{i}^{s}_{i,abc}(t) - \underline{i}^{s}_{g,abc}(t)\right] \\
\frac{d}{dt}\underline{i}^{s}_{g,abc}(t) = \frac{1}{L_2}\left[\underline{v}^{s}_{cf,abc}(t) - \underline{v}^{s}_{g,abc}(t)\right]
\end{cases} \tag{9}$$

Three-phase GCI model in stationary reference frame (*abc* model) is transformed into *dq* model in synchronous reference frame. Although controller can be built on *abc* model in stationary reference frame, using *dq* model is beneficial because state variables at fundamental excitation frequency are dc quantities. This allows PI controller to operate easily to achieve the desired performance.

By using scalar notation, (8) is represented as *dq* model as shown in (10). Block diagram of *dq* model of GCI using scalar notation is shown in Fig. 3 in synchronous *dq* reference frame.

$$\begin{cases}
\frac{d}{dt}i_{i,d}(t) = +\omega i_{i,q}(t) + \frac{1}{L_1}\left[v_{i,d}(t) - v_{cf,d}(t)\right] \\
\frac{d}{dt}v_{cf,d}(t) = +\omega v_{cf,q}(t) - \omega R_d\left[i_{i,q}(t) - i_{g,q}(t)\right] \\
\qquad\qquad + \left(\frac{1}{C_f} + R_d\frac{d}{dt}\right)\left[i_{i,d}(t) - i_{g,d}(t)\right] \\
\frac{d}{dt}i_{g,d}(t) = +\omega i_{g,q}(t) + \frac{1}{L_2}\left[v_{cf,d}(t) - v_{g,d}(t)\right]
\end{cases} \tag{10}$$

$$\begin{cases}
\frac{d}{dt}i_{i,q}(t) = -\omega i_{i,d}(t) + \frac{1}{L_1}\left[v_{i,q}(t) - v_{cf,q}(t)\right] \\
\frac{d}{dt}v_{cf,q}(t) = -\omega v_{cf,d}(t) + \omega R_d\left[i_{i,d}(t) - i_{g,d}(t)\right] \\
\qquad\qquad + \left(\frac{1}{C_f} + R_d\frac{d}{dt}\right)\left[i_{i,q}(t) - i_{g,q}(t)\right] \\
\frac{d}{dt}i_{g,q}(t) = -\omega i_{g,d}(t) + \frac{1}{L_2}\left[v_{cf,q}(t) - v_{g,q}(t)\right]
\end{cases}$$

Conventional double loop PI controller for d-axis and q-axis grid current is designed based on GCI model in (10). There are coupling terms involving angular frequency, ω, between d and q components for every equation and these coupling terms are shown with orange-colored blocks in Fig. 3. There are 6 state variables, 4 inputs, and 2 output variables. Because models for d-axis and q-axis component of the system are separated and there exists coupling term between these two of components, model is complicated and controller should be designed considering four different responses: d-

axis grid current with respect to d-axis inverter voltage, d-axis grid current with respect to q-axis inverter voltage, q-axis grid current with respect to d-axis inverter voltage, and q-axis grid current with respect to q-axis inverter voltage.

Using (6), (9) can be transformed into *dq* model of three-phase GCI with LCL output filter as complex vector in synchronous *dq* reference frame as shown in (11) where superscript *e* represents synchronous *dq* reference frame and bar under variable means complex space vector. A synchronous angular frequency, ω, is $2\pi f_g$ that system is synchronized to the grid.

Fig. 4 is block diagram of *dq* model of three-phase GCI using complex vector notation representing (11). Coupling terms involving ω between *d*- and *q*-axis components of state variables using scalar notation in Fig. 3 are presented as coupling terms involving $j\omega$ (orange-colored one) as shown in Fig. 4. There are 3 state variables, 2 inputs, and 1 output variable when complex vector notation is used.

Comparing *dq* model using scalar notation (10) in Fig. 3 and using complex vector notation (11) in Fig. 4, the use of complex vector notation reduces the number of state variables from 6 to 3, inputs from 4 to 2, and outputs from 2 to 1.

$$\begin{cases} \dfrac{d}{dt}\underline{i}_{i,dq}^{e}(t) = -j\omega\underline{i}_{i,dq}^{e}(t) + \dfrac{1}{L_1}\left[\underline{v}_{i,dq}^{e}(t) - \underline{v}_{cf,dq}^{e}(t)\right] \\ \dfrac{d}{dt}\underline{v}_{cf,dq}^{e}(t) = -j\omega\underline{v}_{cf,dq}^{e}(t) + j\omega R_d\left[\underline{i}_{i,dq}^{e}(t) - \underline{i}_{g,dq}^{e}(t)\right] + \left(\dfrac{1}{C_f} + R_d\dfrac{d}{dt}\right)\left[\underline{i}_{i,dq}^{e}(t) - \underline{i}_{g,dq}^{e}(t)\right] \\ \dfrac{d}{dt}\underline{i}_{g,dq}^{e}(t) = -j\omega\underline{i}_{g,dq}^{e}(t) + \dfrac{1}{L_2}\left[\underline{v}_{cf,dq}^{e}(t) - \underline{v}_{g,dq}^{e}(t)\right] \end{cases} \tag{11}$$

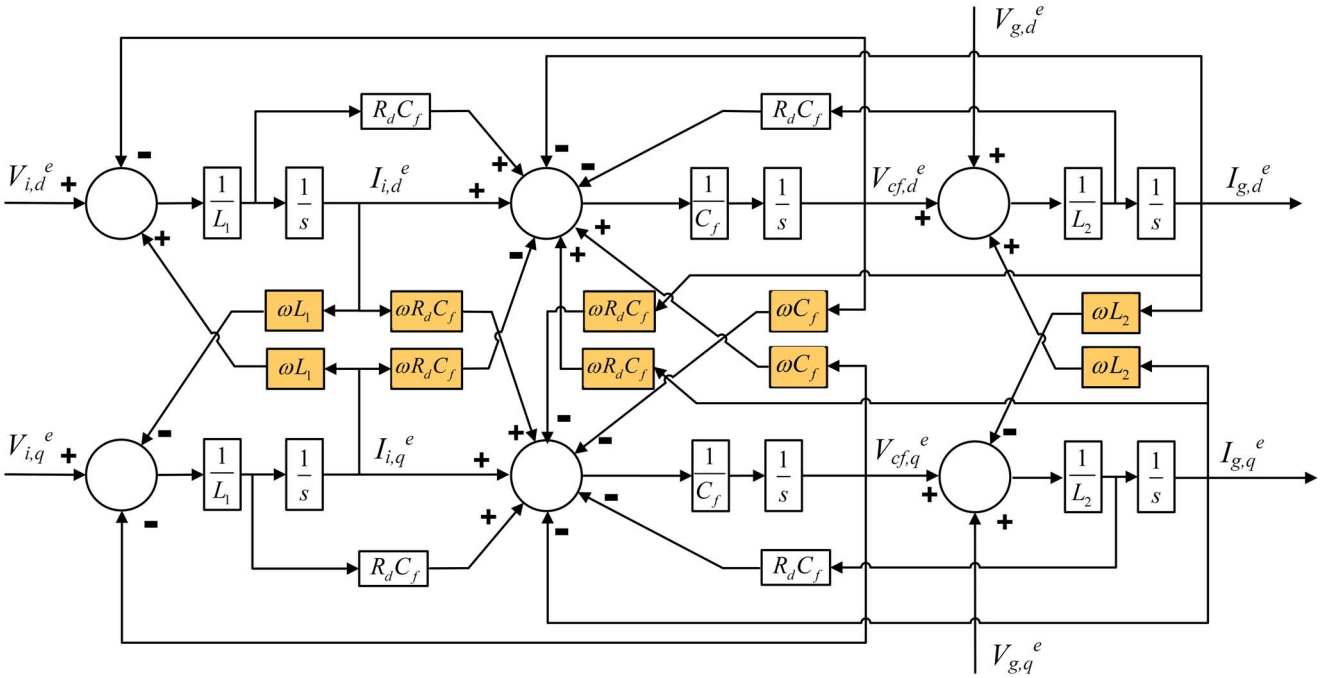

Fig. 3. Block diagram of scalar model of three-phase GCI including LCL output filter in synchronous *dq* reference frame.

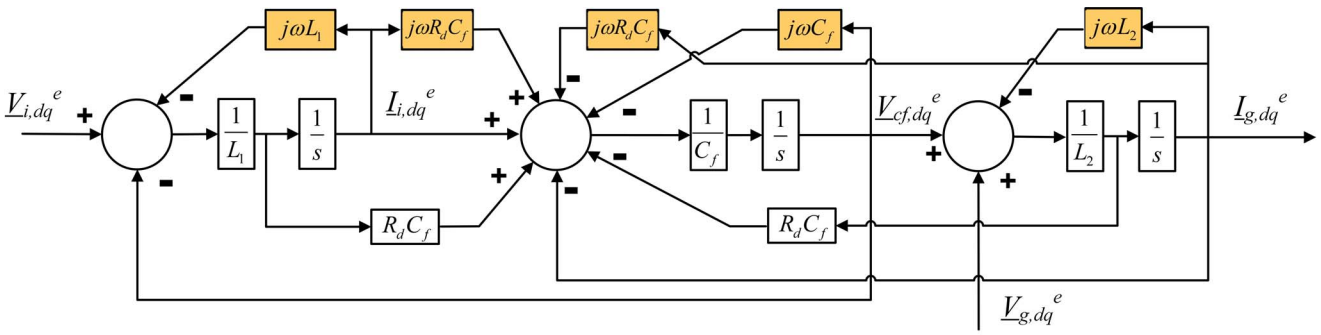

Fig. 4. Block diagram of complex vector model of three-phase GCI including LCL output filter and the grid in synchronous *dq* reference frame.

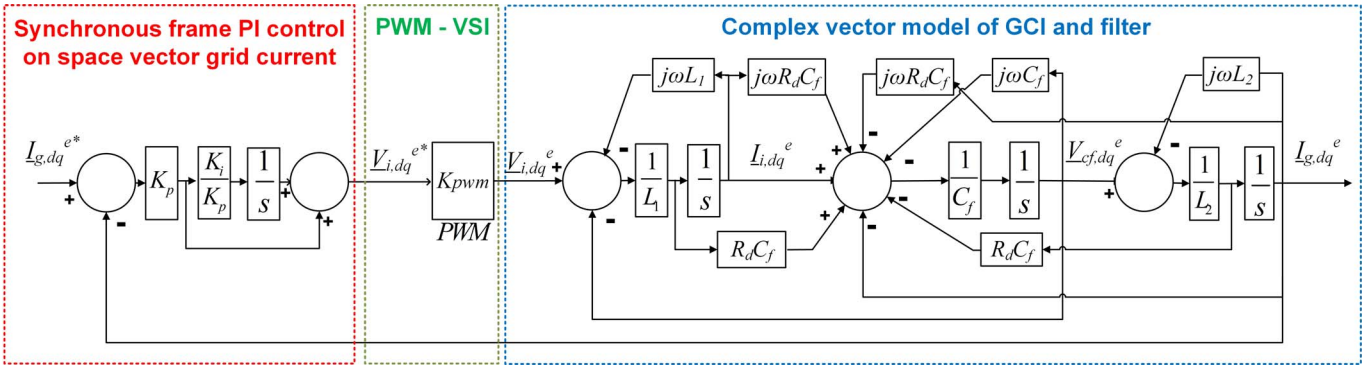

Fig. 5. Block diagram of complex vector GCI model in synchronous *dq* reference frame with synchronous reference PI controller.

Modeling as complex vector gives reduced order of the system and the number of inputs and outputs of the system becomes half of the one when scalar notation is used [9]. The *dq* model of GCI becomes simple when modeled as complex vector and it is easier to design controller and tune the gain of the controller.

Equation (11) can be represented in s-domain and frequency response of complex vector of grid current, $\underline{I}_{g,dq}^{e}$, can be expressed as combination of $\underline{V}_{i,dq}^{e}$ and $\underline{V}_{g,dq}^{e}$. Organizing and solving (11) for grid current with respect to inverter output voltage and grid voltage gives (12)

$$\underline{I}_{g,dq}^{e}(s) = H_1(s)\underline{V}_{i,dq}^{e}(s) + H_2(s)\underline{V}_{g,dq}^{e}(s) \tag{12}$$

where $H_1(s)$ is written as

$$H_1(s) = \frac{1}{L_1}\frac{Z_{LC}^2}{\omega_{res}}\frac{1}{(s+j\omega)}\frac{s+\omega_{res}+j\omega}{D(s)}$$
$$D(s) = s^2 + (\omega_{res}+j2\omega)s + (\omega_{res}^2 - \omega^2 + j\omega_{res}\omega) \tag{13}$$

and $H_2(s)$ is expressed as

$$H_2(s) = \frac{1}{L_2}\frac{1}{(s+j\omega)}\frac{N(s)}{D(s)}$$
$$N(s) = s^2 + \left(\frac{R_d}{L_1}+j2\omega\right)s + \left(-\omega^2 + \frac{1}{L_1C_f} + j\frac{R_d}{L_1}\omega\right) \tag{14}$$

Square of resonant angular frequency is defined as

$$\omega_{res}^2 = \frac{L_1+L_2}{L_1L_2C_f} \tag{15}$$

Square of impedance regarding L_2 and C_f is

$$Z_{LC}^2 = \frac{1}{L_2C_f} \tag{16}$$

Damping resistance of output filter is

$$R_d = \frac{1}{\omega_{res}C_f} \tag{17}$$

Poles of open loop system are located at $s = -0.5\omega_{res} - j\left(\omega \pm \left(\sqrt{3}/2\right)\omega_{res}\right)$, $-j\omega$. These poles are unsymmetrical with respect to imaginary axis of complex plane because transfer function involves the coefficients, which are complex.

To regulate current-controlled GCI in synchronous *dq* reference frame, synchronous frame PI controller is implemented as shown in Fig. 5. Synchronous frame PI controller is modeled as

$$\underline{V}_{g,dq}^{e}(s) \approx K_p\left(\frac{s+K_i/K_p}{s}\right)\left(\underline{I}_{g,dq}^{e*}(s) - \underline{I}_{g,dq}^{e}(s)\right) \tag{18}$$

Conventionally, there are sensors for the dc link voltage, three-phase grid current, and three-phase PCC voltage. PCC voltage is fed back to phase lock loop (PLL) for grid synchronization.

In this paper, dc link voltage, three-phase grid current, and three-phase grid voltage are sensed because PCC voltage is the same as grid voltage when grid impedance is neglected. K_{pwm} is defined as the gain of PWM of voltage source inverter and assumed to be unity.

Substituting (18) into (12) gives closed loop transfer function of grid current with respect to command of grid current represented in synchronous *dq* reference frame as expressed

$$\frac{\underline{I}_{g,dq}^{e}(s)}{\underline{I}_{g,dq}^{e*}(s)} = \frac{1}{L_1}\frac{Z_{LC}^2}{\omega_{res}}K_p\frac{s^2+N_1s+N_0}{s^4+D_3s^3+D_2s^2+D_1s+D_0} \tag{19}$$

where

$$N_1 = \frac{K_i}{K_p} + \omega_{res} + j\omega$$
$$N_0 = \frac{K_i}{K_p}(\omega_{res}+j\omega)$$
$$D_3 = \omega_{res} + j3\omega$$
$$D_2 = \omega_{res}^2 - 3\omega^2 + j2\omega\omega_{res} + \frac{1}{L_1}\frac{Z_{LC}^2}{\omega_{res}}K_p$$

$$D_1 = \omega\left\{-\omega_{res}\omega + j\left(\omega_{res}^2 - \omega^2\right)\right\} + \frac{1}{L_1}\frac{Z_{LC}^2}{\omega_{res}}\left\{K_i + K_p\left(\omega_{res} + j\omega\right)\right\}$$

$$D_0 = \frac{1}{L_1}\frac{Z_{LC}^2}{\omega_{res}}K_i\left(\omega_{res} + j\omega\right)$$

IV. Analytical and Simulation Results of GCI, and Effect of Tuning Parameter of PI Controller

Analytical results of closed loop transfer function of grid current are presented in this section. Complex vector root locus and frequency response function for different PI controller's gains are shown.

The specification of the grid, inverter, and LCL output filter is shown in Table I. LCL output filter is designed for 10 kW of rated power of IGBT inverter with 6 kHz of switching frequency when line-to-line grid voltage is 240 Vrms. Considering maximum 5 % of reactive power consumed by LCL filter, shunt connected filter capacitor is set to be 20 uF. Rest of parameters of output filter is shown in Table I. Resonance at 2.05 kHz due to the LCL filter is mitigated by passive damping resistor.

TABLE I. Specification of the Grid and Output Filter

Grid		**LCL Output Filter**	
Grid voltage, V_g	240 Vrms	Inverter-side inductance, L_1	990 μH
Grid frequency, f_g	60 Hz	Grid-side inductance, L_2	430 μH
Grid resistance, R_g	0 pu (stiff)	Shunt filter capacitance, C_f	20 μF
Grid inductance, L_g	0 pu (stiff)	Damping resistance, R_d	3.5 Ω

Open loop poles are located at -6,457 - *j*11,561, -6,457 + *j*10,807, and –*j*377. Zero of open loop system is at -12,914 + *j*377.

Fig. 6 shows trajectories of complex vector root locus of GCI in synchronous *dq* reference frame for different K_i/K_p. K_i/K_p is location of zero of PI controller. Root locus is examined when K_i/K_p is 20, 200, and 2,000. Open loop poles are located far from origin so that zoomed root locus around origin is shown in right column of figure. Trajectories of open loop including additional pole of PI controller at origin are shown as the same color as K_p is increasing. There are four closed loop poles migrating as K_p increases from 0 to 1000. As GCI is modeled using complex vector notation, poles are unsymmetrical about the imaginary axis. Poles of GCI are located in stable region for all K_p value when K_i/K_p is 20 and 200 as shown in Fig. 6 (a) and (b). For 2,000 of K_i/K_p, system becomes unstable when K_p is larger than 102. Open loop pole at –j377 migrates to zero of PI controller and becomes dominant closed loop pole. Therefore, K_i/K_p is important tuning parameter that contributes to bandwidth of the system.

Frequency responses of complex vector model of GCI are shown in Fig. 7 according to different K_i/K_p and K_p. Frequency response of grid current with respect to command of grid current is plotted for 20, 200, and 2,000 of K_i/K_p. Equation (18) is plotted for frequency range from -1,000 Hz to 1,000 Hz, which presents negative frequency to positive frequency. Gain K_p is selected to be 5, 10, 20, 50, and 100.

Frequency response shows complex vector of grid current consisting of d- and q-axis component with respect to command in synchronous *dq* reference frame, which is shown in (19). Magnitude and phase of frequency response of complex vector grid current are 1 and 0, respectively, when frequency is 0. This is because *dq* model is presented in synchronous *dq* reference frame. The meaning of frequency response function is how the system would response to command components at non-zero frequency. In other words, Fig. 7 shows how well grid current is regulated so that undesired grid current caused by disturbance of command at non-zero frequency is well attenuated. Disturbance of command grid current at non-zero frequency has more effects on grid current as magnitude of frequency response is closer to unity value in entire frequency range except for non-zero frequencies. Magnitude of frequency response of grid current should be less than 1 at non-zero frequency. Therefore, undesired grid current caused by undesired command would be attenuated.

In Fig. 7 (a) when K_i/K_p is 20, grid current is better regulated for 5 and 10 of K_p than one for 20, 50, and 100 of K_p. Case of K_p = 5 performs better than other K_p values even though there is overshoot at f = 50 Hz. For K_i/K_p = 20 and K_p = 5, closed loop poles are located at –4,832 – j12,924, –4,832 + j12,170, –3,230 – j379, and –20 + j2. Fig. 7 (b) is frequency response of grid current when K_i/K_p is 200. Overall response is similar to responses when K_i/K_p is 20. However, response has larger overshoot at f = 40 Hz than one when K_i/K_p is 20. For K_i/K_p = 200 and K_p = 5, closed loop poles are located at –4,818 – j12,900, –4,818 + j12,144, –3,068 – j401, and –210 + j25. Frequency response when K_i/K_p is 2000 is different from one when K_i/K_p is 20 and 200. Only K_p = 5 case performs well in spite of larger overshoot at 320 Hz. When K_p is 100, which is larger than the maximum K_p value, 102, to avoid instability, frequency response shows that system cannot attenuate undesired component of command at non-zero frequencies. For K_i/K_p = 2,000 and K_p = 100, closed loop poles are located at 44 – j34,230, 63 + j33,476 , –10,966 – j389, and –2,056 + j12.

Fig. 7 shows one of benefits that complex vector model has on analysis and characterization of system and controller's tuning parameters. Complex vector model enables to analyze just one plot of frequency response, whereas four plots of frequency response (I_g^d/I_g^{d*}, I_g^d/I_g^{q*}, I_g^q/I_g^{d*}, and I_g^q/I_g^{q*}) should be analyzed when using scalar model.

Fig. 8 shows step responses of complex vector modeled GCI represented in synchronous *dq* reference frame for different K_p gain values when K_i/K_p is 20, 200, and 2,000. Command grid current steps up to 1 when time is 0. Corresponding to results in Fig. 7, grid current is well regulated and shows over-damped response for 5 of K_p. Grid

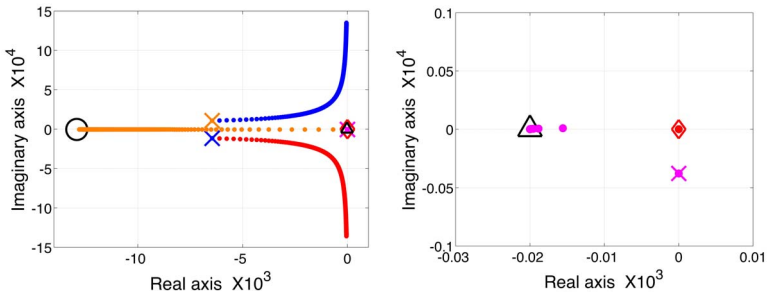

(a) $K_i/K_p = 20$

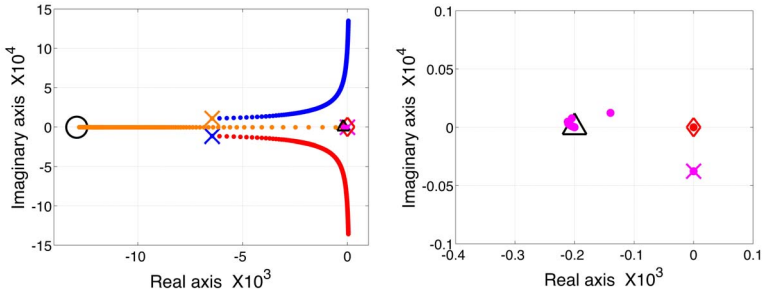

(b) $K_i/K_p = 200$

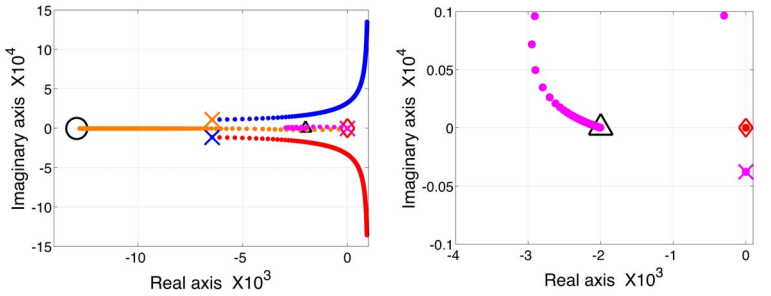

(c) $K_i/K_p = 2{,}000$

Fig. 6. Complex vector root locus of GCI represented in synchronous *dq* reference frame for different K_i/K_p, figures in right column are zoomed figures in left column, K_p is increasing from 0 to 1000, open loop pole: X X X, Open loop zero: O, PI controller's pole at origin: ◆, PI controller's zero at K_i/K_p: Δ.

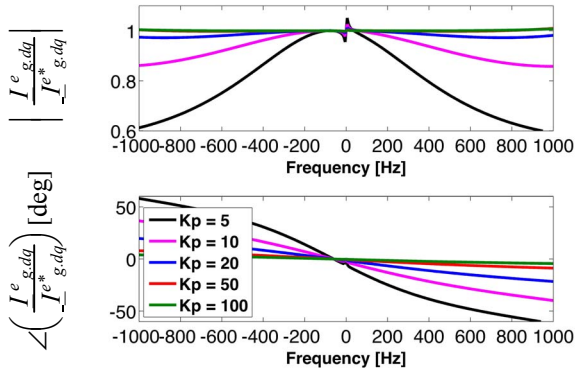

(a) $K_i/K_p = 20$

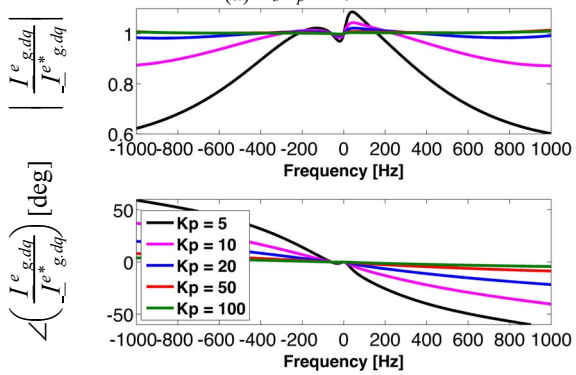

(b) $K_i/K_p = 200$

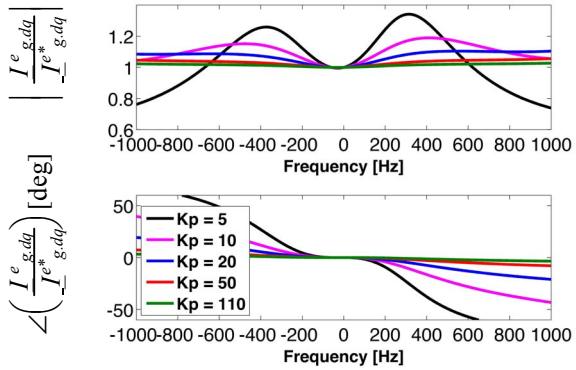

(c) $K_i/K_p = 2{,}000$

Fig. 7. Frequency response function of GCI represented in synchronous *dq* reference frame for different K_i/K_p *and* K_p.

current is under-damped when K_p is larger than 10. Setting time increases as K_p increases. System is damped and takes the longest time to become steady-state value when K_p is 100. A step response of grid current when K_i/K_p is 200 is similar to the one when K_i/K_p is 20. When K_i/K_p is 2000, step response for 5 of K_p is under-damped, but setting time is longer than one when K_i/K_p is 20 and 200. Also, step response diverges when K_p is 110, which is a corresponding result shown in Fig. 7 (c), that the system becomes unstable.

Fig. 8 is also showing advantages of using complex vector model that just one plot of step response is needed to see performance of PI controller and analyze controller's tuning parameter on system performance.

A 10 kW GCI with synchronous frame PI controller is simulated using MATLAB Simulink with SimPowerSystems ™. GCI is regulated when tuning parameters, K_i/K_p and K_p, are 200 and 5, respectively. Results are shown in Fig. 9.

V. Conclusion

This paper presents the modeling, using complex vectors, of three-phase GCI with LCL filter and the grid when grid current is regulated using synchronous frame PI controller. Controller is designed on complex vector of grid current in synchronous *dq* reference frame. Closed loop function of complex vector of grid current with respect to complex vector

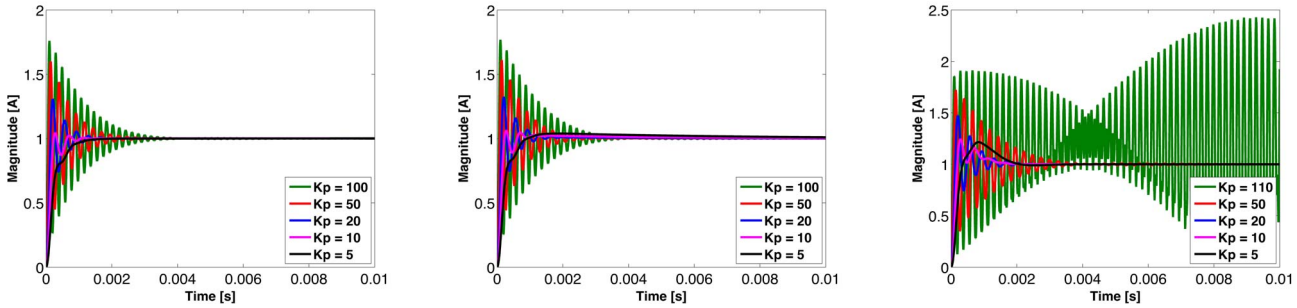

(a) $K_i/K_p = 20$ (b) $K_i/K_p = 200$ (c) $K_i/K_p = 2{,}000$

Fig. 8. Magnitude of step response of complex vector modeled GCI represented in synchronous *dq* reference frame for different K_i/K_p *and* K_p.

of command current is derived including synchronous frame PI controller.

Complex vector model of GCI has benefits of reduced order of GCI system from 6th to 3rd order and simple structure that two separate block diagram for d- and q-axis component can be represented in one single block diagram. Performance of PI controller and effect of tuning parameter is examined using complex vector root locus and complex vector frequency response function. Complex vector model enables that system performance can be examined using just single plot of root locus and frequency response function. For 10 kW three-phase grid-connected inverter and given specification, optimal tuning parameter for K_i/K_p = 20 and 200 is K_p = 5. Step response of system and the simulated results using MATLAB are also presented. Complex vector model based on physical system is beneficial to tune gain parameters of synchronous PI controller rather than trial and error.

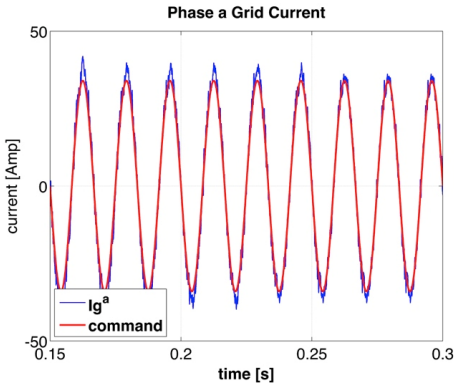

Fig. 9. Phase A grid current of three-phase GCI with synchronous frame PI controller (K_i/K_p is 200, K_p is 5).

ACKNOWLEDGMENT

This research has been funded in part by the DOE Sunshot Initiative under award DE-0006341.

REFERENCES

[1] R. Teodorescu, M. Liserre, and P. Rodríguez, *Grid Converters for Photovoltaic and Wind Power Systems*: John Wiley & Sons, Ltd, 2011.

[2] L. Poh Chiang and D. G. Holmes, "Analysis of multiloop control strategies for LC/CL/LCL-filtered voltage-source and current-source inverters," *IEEE Trans. Ind. Appl.,* vol. 41, no. 2, pp. 644-654, 2005.

[3] L. Poh Chiang, M. J. Newman, D. N. Zmood, and D. G. Holmes, "A comparative analysis of multiloop voltage regulation strategies for single and three-phase UPS systems," *IEEE Trans. Power Electron.,* vol. 18, no. 5, pp. 1176-1185, 2003.

[4] D. N. Zmood, D. G. Holmes, and G. H. Bode, "Frequency-domain analysis of three-phase linear current regulators," *IEEE Trans. Ind. Appl.,* vol. 37, no. 2, pp. 601-610, 2001.

[5] J. Dannehl, C. Wessels, and F. W. Fuchs, "Limitations of voltage-oriented PI current control of grid-connected PWM rectifiers with LCL filters," *IEEE Trans. Ind. Electron.,* vol. 56, no. 2, pp. 380-388, 2009.

[6] D. N. Zmood and D. G. Holmes, "Stationary frame current regulation of PWM inverters with zero steady-state error," *IEEE Trans. Power Electron.,* vol. 18, no. 3, pp. 814-822, 2003.

[7] T. Erika and D. G. Holmes, "Grid current regulation of a three-phase voltage source inverter with an LCL input filter," *IEEE Trans. Power Electron.,* vol. 18, no. 3, pp. 888-895, 2003.

[8] F. B. Del Blanco, M. W. Degner, and R. D. Lorenz, "Dynamic analysis of current regulators for AC motors using complex vectors," *IEEE Trans. Ind. Appl.,* vol. 35, no. 6, pp. 1424-1432, 1999.

[9] F. Briz, M. W. Degner, and R. D. Lorenz, "Analysis and design of current regulators using complex vectors," *IEEE Trans. Ind. Appl.,* vol. 36, no. 3, pp. 817-825, 2000.

[10] K. Hyunbae and R. D. Lorenz, "Synchronous frame PI current regulators in a virtually translated system," in *Conf. Rec. 2004 IEEE IAS Ann. Meeting*, 2004, pp. 856-863.

[11] M. Prodanovic and T. C. Green, "Control and filter design of three-phase inverters for high power quality grid connection," *IEEE Trans. Power Electron.,* vol. 18, no. 1, pp. 373-380, 2003.

[12] J. Dannehl, F. W. Fuchs, and P. B. Thogersen, "PI state space current control of grid-connected PWM converters with LCL filters," *IEEE Trans. Power Electron.,* vol. 25, no. 9, pp. 2320-2330, 2010.

[13] F. Blaabjerg, R. Teodorescu, M. Liserre, and A. V. Timbus, "Overview of control and grid synchronization for distributed power generation systems," *IEEE Trans. Ind. Electron.,* vol. 53, no. 5, pp. 1398-1409, 2006.